Materials Science and Engineering A 397 (2005) 310–313

www.elsevier.com/locate/msea

A quantitative analysis of the chlorination of samarium sesquioxide

M.R Esquivel [a,*], A.E Bohé [b], D.M. Pasquevich [a,b]

[a] *Centro Atómico Bariloche-Comisión Nacional de Energía Atómica, S.C. de Bariloche, R8402AGP Río Negro, Argentina*

[b] *Consejo Nacional de Investigaciones Científicas y Técnicas, S.C. de Bariloche, R8402AGP Río Negro, Argentina*

Received 20 October 2004; received in revised form 10 February 2005; accepted 28 February 2005

Abstract

In this work, the experimental data of the chlorination of Sm_2O_3 analyzed previously by thermogravimetry (TG) between 200 and 350 °C is fitted using the equations of Johnson–Mehl–Avrami (JMA). The presence of a change of the apparent activation energy (E_{ap}) is correlated to a change on the parameters (n and k) of the JMA model. The values of n found were 1/2 and 2/3 in the 200–270 and 270–350 °C, respectively. These values were correlated to a change on the mechanism of the reaction. The k values obtained from the JMA equations were used to confirm the experimental E_{ap} values previously found in the mentioned higher and lower temperature range: 45 ± 5 and 130 ± 5 kJ mol^{-1}, respectively. The nucleation and growth processes observed were also in agreement with results obtained by scanning electron microscopy (SEM), energy dispersive spectroscopy (EDS) and X-ray diffraction (XRD).
© 2005 Elsevier B.V. All rights reserved.

Keywords: Modeling; JMA; Chlorination; Samarium oxide

1. Introduction

The synthesis and isolation of different lanthanide oxychlorides from either synthetic or natural lanthanide oxide mixtures constitutes a field of interest due to the many applications of these compounds in luminescence and optics [1,2]. Many of the advantages of the oxychlorides are related to their stability at room temperature, which facilitates their storage and handling.

Like those of the other compounds of lanthanides, the microstructure and properties of the obtained SmOCl depend on the kind of precursor and temperature of synthesis used. This compound can be obtained by direct chlorination of Sm_2O_3 present as such or as a constituent of oxide mixtures [3,4]. This process leads to the formation of SmOCl according to the following stoichiometry in the 190–950 °C temperature range [4]:

$$Sm_2O_3(s) + Cl_2(g) = 2SmOCl(s) + \tfrac{1}{2}O_2(g) \quad (1)$$

At high temperatures, from 950 to 350 °C, external mass transfer influences the reaction rate. Between 350 and 200 °C, the chlorination progresses slowly under mixed chemical and transport control [4]. In this temperature range, the formation of the oxychloride is thought to be achieved by nucleation and growth over the particles of the initial oxide [4]. Since both the size and microstructure of the particles obtained are dependent of the conditions and temperature of synthesis, a further analysis of this process is done in order to determine the conditions under which a controlled growth of the particles of SmOCl can be obtained. In this work, a first approximation to the quantitative analysis of the chlorination of Sm_2O_3 in the 200 °C to 350 °C temperature range is reported. The evolution of the reaction is modeled according to the equations of Mehl-Johnson-Avrami (JMA) [5–8]. The chlorination for growth of potential precursors such as SmOCl is used in the industrial field and the present work augments scientific knowledge.

* Corresponding author. Tel.: +54 2944 445100/5132; fax: +54 2944 445299.
E-mail address: esquivel@cab.cnea.gov.ar (M.R Esquivel).

0921-5093/$ – see front matter © 2005 Elsevier B.V. All rights reserved.
doi:10.1016/j.msea.2005.02.061

2. Data presentation

The temporal evolution of the reaction (1) previously analyzed [4] can be represented by:

$$\alpha_{Sm_2O_3} = f\frac{\Delta m}{m_0} \quad (2)$$

where $\alpha_{Sm_2O_3}$, Δm, m_0 and f stand for reaction degree, Sm_2O_3 mass change, initial Sm_2O_3 mass and a stoichiometric coefficient that correlates the mass change on the electrobalance used to measure this reaction [4]. In this case, this coefficient is equal to 6.36.

3. Results and discussion

3.1. Characteristics of the reaction and its relationship with nucleation and growth processes

The progress of the reaction represented by Eq. (1) [4] can be observed in Fig. 1. In this figure, an experimental TG curve of the reaction at 300 °C is shown [4]. A marked "s" shaped form on the curve can be seen. This behavior is repeated in all the experiments conducted within the 200–350 °C temperature range [4]. This is an indication that the reaction progresses under nucleation and growth processes [9,10].

SEM images of the initial Sm_2O_3 and final product SmOCl are shown in the left upper inset and the right lower inset of Fig. 1, respectively. SmOCl particles were also identified by EDS.

The experimental diffraction patterns of the products of reaction obtained at various $\alpha_{Sm_2O_3}$ (Fig. 2(A–D)) along with the reference patterns of both Sm_2O_3 [11] and SmOCl [12] are reported in Fig. 2. No other products such as $SmCl_3$ [13], $SmCl_2$ [13], Sm_4OCl_6 [14] or Sm_3Cl_7 [15] were found. No reduced oxides such as SmO were detected [16].

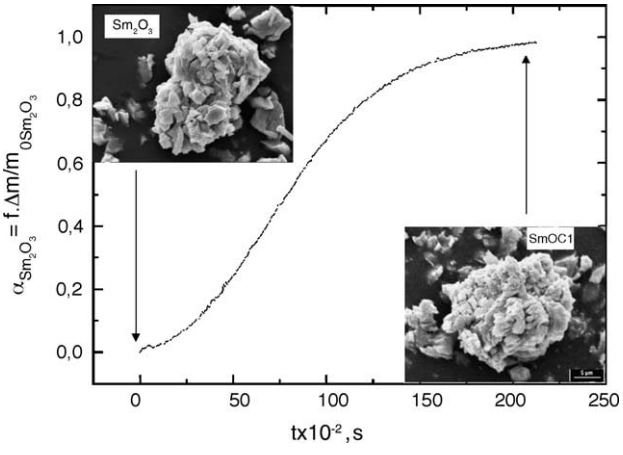

Fig. 1. A characteristic TG curve for this reaction at 300 °C [4]. A marked "s" shape is observed. The left upper inset shows a SEM image of the initial Sm_2O_3. The right lower inset shows a SEM image of the obtained SmOCl. This last compound was also identified by EDS.

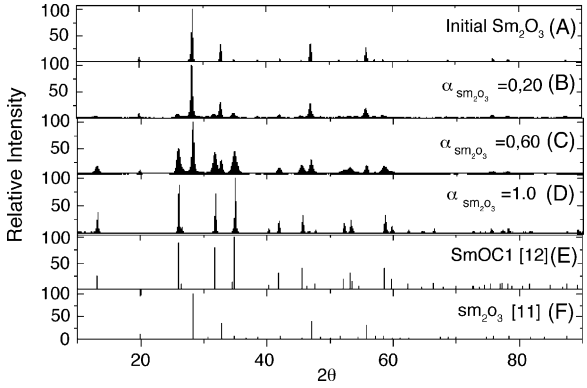

Fig. 2. Diffraction patterns of the reaction products at 300 °C at various $\alpha_{Sm_2O_3}$: (A) $\alpha_{Sm_2O_3} = 0.0$, (B) $\alpha_{Sm_2O_3} = 0.2$, (C) $\alpha_{Sm_2O_3} = 0.6$, (D) $\alpha_{Sm_2O_3} = 1.0$, (E) reference pattern of SmOCl [12] and (F) reference pattern of Sm_2O_3 [11].

The strong morphological similarities between both initial Sm_2O_3 and final SmOCl plate like particles observed in the insets of Fig. 1 and the fact that no other phases were observed at intermediate $\alpha_{Sm_2O_3}$ (Fig. 2) also supports the assumption that the temporal evolution of the reaction is achieved by nucleation and growth of the solid SmOCl over the solid Sm_2O_3.

3.2. Application of the JMA equations

The parameter that represents the fraction of the phase transformed is $\alpha_{Sm_2O_3}$ which is defined by Eq. (2). This is reasonable because no phase other than SmOCl was detected (over Sm_2O_3) as described in the previous section. Then, the nucleation and growth of this new phase can be represented by the JMA model [5–8]. This model assumes that the nucleation is either constant or a maximum at the beginning of the transformation and decreases during this process [5–6]. The following equation represents this behavior:

$$\alpha_{Sm_2O_3} = 1 - \exp(kt^n) \quad (3)$$

In this equation, t stands for the time of transformation and k and n are parameters that depend on the mechanism of transformation. The values of n are correlated to the morphology and mechanism of the growth [17].

3.3. Fitting of the data obtained previously [4]

To determine the n and k parameters involved in Eq. (3), the experimental data was evaluated using different integrated Avrami–Mampel–Erofeev equations [17] considering nucleation and growth as rate limiting process, growth rate being determined by the chemical reaction at the boundary of the growing nucleus [17] and growth rate being limited by diffusion from the phase boundary to the surface [17] according the following expression:

$$kt = n(-\ln(1-\alpha))^n \quad (4)$$

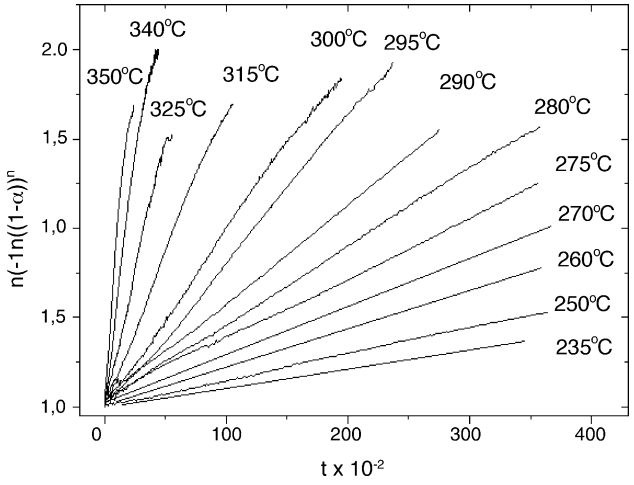

Fig. 3. Fitting of the experimental data obtained in a previous work [4] using Eq (4). The values of n found for TG curves under and over 270 °C correspond to 1/2 and 2/3, respectively. The corresponding R-correlation values for each curve are displayed in the third column of Table 1.

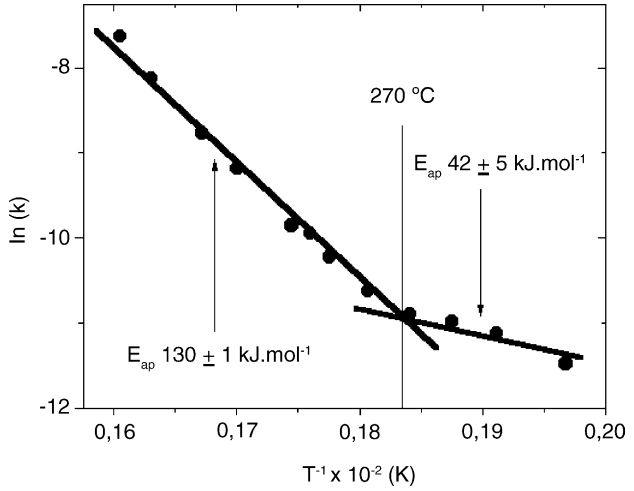

Fig. 4. Calculation of the E_{ap} in the 350–200 °C temperature range using the values of k displayed in Table 1.

The fitting of the experimental data [4] using Eq. (4) is displayed in Fig. 3.

The best fitting for curves between 200 and 270 °C is achieved with $n = 2/3$. For curves between 270 and 350 °C, the best fitting is achieved with $n = 1/2$. The k values obtained at each temperature are displayed in the third column of Table 1.

3.4. The apparent activation values and the evolution of the chlorination

The apparent activation energy (E_{ap}) involved in the process described by Eq (4) using $n = 1/2$ and 2/3 can be calculated if the k values obtained are represented against the inverse of the absolute temperature. The calculation is shown in Fig. 4. Between 350 and 270 °C, an E_{ap} value of 130 ± 1 kJ mol^{-1} is obtained. Between 270 and 200 °C, a E_{ap} value of 45 ± 5 kJ mol^{-1} value is obtained. These values are in agreement with those previously obtained [4].

Table 1
The n and k values obtained at various temperatures in the 270–350 °C temperature range from fitting of the curves shown in Fig. 3 using Eq. (4)

T (°C)	n	k (s^{-1})	R
350	1/2	4.48×10^{-4}	0.993
340	1/2	2.96×10^{-4}	0.997
325	1/2	1.55×10^{-4}	0.998
315	1/2	8.79×10^{-4}	0.998
300	1/2	5.24×10^{-5}	0.998
290	1/2	3.78×10^{-5}	0.999
280	1/2	3.00×10^{-5}	0.999
270	2/3	2.93×10^{-5}	0.999
260	2/3	1.79×10^{-5}	0.999
250	2/3	1.47×10^{-5}	0.999
235	2/3	1.03×10^{-5}	0.999

R corresponds to the minimum-squares correlation coefficient of the curves shown in Fig. 3.

The diminution of the E_{ap} as temperature increases suggests that the reaction is selecting an alternative process between reactions in parallel [18]. At the higher temperature range, the parameter n found equal to 1/2 suggests that both nucleation and growth are the limiting processes. In this case, the rate of growth is limited by the chemical reaction, which is produced within the boundaries of the growing nucleus [17]. The global process is achieved under an E_{ap} of 130 ± 1 kJ mol^{-1}. At the lower temperature range, the value n found (2/3) suggest that the reaction is controlled by growth which global rate is controlled by the diffusion rate from the boundary of the phase to the surface [18]. This last process is correlated with the increment in the depth of the sample (since SmOCl is deposited over unreacted Sm_2O_3) and the distance of contact between the particles of the sample. Since both processes are affected by the intrinsic chemical reaction, the values of E_{ap} obtained were assigned to the global process.

4. Conclusions

In this work, a further analysis of the chlorination of Sm_2O_3 [4] is performed. Complementary analyses of the reaction products to those previously studied [4] were used to confirm that SmOCl(s) is nucleated over Sm_2O_3(s). The nucleation and growth processes observed were fitted using the JMA equations. The parameters obtained from these equations were used both to define the form that nucleation and growth evolve in this reaction and to confirm previous results on the E_{ap} values [4]. The increment on the E_{ap} values as temperature raises is associated to a change of the mechanism of reaction between parallel paths.

In the 200–270 °C temperature range, the reaction is controlled by growth of the nucleus which global rate is controlled by the rate of diffusion from the boundary of the phase to the surface under a global E_{ap} of 45 ± 5 kJ mol^{-1}.

In the 270–350 °C temperature range, the reaction is limited by both nucleation and growth. In this case, the rate of growth is limited by the chemical reaction, which is produced within the boundaries of the growing nucleus. In this case, the reaction evolves under a global E_{ap} of $130 \pm 1\,kJ\,mol^{-1}$.

References

[1] S. Areva, J. Hölsä, R.J. Lamirnäki, H. Rahiala, P. Deren, W. Strek, J. Alloys Compd. 300–301 (2000) 218–223.
[2] U. Rambabu, K. Ramahojan Reddy, K. Annapurna, T. Balaji, J.V. Satyanarayana, S. Buddhuhu, Mater. Lett. 27 (1996) 59–63.
[3] M.R. Esquivel, A.E. Bohé, D.M. Pasquevich, in: J.P. Barbosa, A.J. Dutra, R. Melamed, R. Trindade (Eds.), Proceedings of the Sixth Southern Hemisphere Meeting on Mineral Technology, vol. 2, 2001, pp. 468–474.
[4] M.R. Esquivel, A.E. Bohé, D.M. Pasquevich, submitted for publication.
[5] W. Johnson, R. Mehl, Trans. AIME 135 (1939) 1103.
[6] M.J. Avrami, J. Chem. Phys. 7 (1939) 1103.
[7] M.J. Avrami, J. Chem. Phys. 8 (1940) 212.
[8] M.J. Avrami, J. Chem. Phys. 7 (1941) 177.
[9] M.E. Brown, A. Knox Galwey, Thermochim. Acta 29 (1979) 129–146.
[10] J. Beretka, J. Am. Ceram. Soc. 67 (1984) 615–619.
[11] Joint Committee for Powder Diffraction Standards, Powder Diffraction File, International Center for Diffraction Data, Swarthmore, PA, 1984 (card number 431029).
[12] Joint Committee for Powder Diffraction Standards, Powder Diffraction File, International Center for Diffraction Data, Swarthmore, PA, 1996 (card number 120790).
[13] D. Brown, Halides of the Lanthanides and Actinides, Wiley/Interscience, London, 1968, pp. 117–181 (Chapter 3).
[14] Joint Committee for Powder Diffraction Standards, Powder Diffraction File, International Center for Diffraction Data, Swarthmore, PA, 1994 (card number 421018).
[15] International Committee Diffraction Data, Powder Diffraction File, Swarthmore, PA, 1994 (card number 440905).
[16] R.G. Haire, L.R. Eyring, Comparisons of the binary oxides, in: K.A. Gschneidner Jr., L. Eyring (Eds.), Handbook of the Physics and Chemistry of the Rare Earths, vol. 18, Elsevier Science Publishers, Amsterdam, 1994, pp. 415–439.
[17] G. Pokol, G. Várhegvi, CRC, Crit. Rev. Anal. Chem. 19 (1988) 65–92.
[18] O. Levenspiel, Chemical Reaction Engineering, vol. 32, Wiley, New York, 1979.